

<http://dx.doi.org/10.1590/2318-0331.0217160021>

## Prediction of the bedforms generated by density currents based on fluvial phase diagrams

### *Previsão das formas de fundo geradas por correntes de densidade a partir de diagramas de fases fluviais*

Débora Karine Koller<sup>1</sup>, Ana Luiza de Oliveira Borges<sup>1</sup>, Eduardo Puhl<sup>1</sup> and Rafael Manica<sup>1</sup>

<sup>1</sup>Universidade Federal do Rio Grande do Sul, Porto Alegre, RS, Brazil

E-mails: debora.koller@ufrgs.br, alborges@iph.ufrgs.br, puhleduardo@gmail.com, rafaelmanica@gmail.com

Received: November 03, 2016 - Revised: April 27, 2017 - Accepted: May 30, 2017

#### ABSTRACT

Density currents, whose movement takes place by the density difference between the flow and the ambient fluid around it, can interact with the substrate generating bedforms similar to the fluvial environments. However, there are no specific bedform phase diagrams capable to predict this type of phenomenon. This study aims to compare the prediction of fluvial bedforms phase diagram with those generated by experimental saline currents. Bedforms were generated in two-dimensional tilting plexiglass flume submerged in a larger tank filled with water with three different mobile beds and varied values of discharge and salt concentration. It was observed three types of bedform (lower plane bed, ripples and dunes), which, with the concomitant calculation of hydrodynamic parameters (mean velocity, energy and mobility) allowed the use of the phase diagram. It was observed that the fluvial phase diagrams did not present good predictions for bedforms generated by density currents. This fact is associated to the hydrodynamics differences (velocity and concentration profiles) and the limitation of the dimensional parameters in the extrapolation of results. Therefore, it is indicated the need to draw up a proper phase diagram to density currents.

**Keywords:** Density current; Bedforms; Physical modeling; Mobile bed; Bedform phase diagram.

#### RESUMO

As correntes de densidade, cujo movimento ocorre pela diferença de massa específica entre o escoamento e o fluido ambiente ao seu redor, podem interagir com o substrato gerando formas de fundo, similares às encontradas em ambientes fluviais. Entretanto não existem diagramas de previsão específicos correspondentes para esse tipo de fenômeno. Assim, este trabalho visa comparar a ocorrência das formas de fundo fluviais previstas nos diagramas de previsão com aquelas geradas por correntes de densidade salinas obtidas experimentalmente. As formas de fundo foram geradas em um canal bidimensional de declividade variável, preenchido por água, com três composições de leito móvel e diferentes valores de vazão, massa específica e inclinação. Três formas de fundo foram identificadas (leito plano inferior, ondulações e dunas), as quais, juntamente com o cálculo de parâmetros hidrodinâmicos permitiram a utilização dos diagramas fluviais. Verificou-se que os diagramas fluviais não apresentaram boas previsões das formas de fundo geradas por correntes de densidade. A esse fato são atribuídas as diferenças hidrodinâmicas dos escoamentos (perfis de velocidade e concentração) e, também, à limitação dos parâmetros dimensionais na extrapolação dos resultados. Dessa forma, indica-se a necessidade de se elaborar um diagrama de previsão próprio adaptado a estas correntes.

**Palavras-chave:** Corrente de densidade; Formas de leito; Modelagem física; Leito móvel; Diagrama de previsão.



## INTRODUCTION

Bedforms are sedimentary features observed in several environments, such as eolian, fluvial, and deep sea, generated by the stresses applied by certain flows.

The understanding on processes of erosion, transport and sedimentation of the grains, which makes up the generation and development of bedforms has been extensively approached by fluvial hydrology for many decades (HJÜSTROM, 1935 apud GRAF, 1971; SHIELDS, 1936; RAUDKIVI, 1997; CARTIGNY; POSTMA, 2016, among others).

Each type of flow develops specific hydraulic characteristics (e.g., velocity and concentration) that are eventually transmitted to the mobile bed over which it flows, such as generating bedforms. Thus, the study of these forms (plane bed, ripples, dunes, and antidunes - SIMONS; RICHARDSON, 1961) can be used as a tool in the understanding of hydraulic processes based on existing geological records in nature, such as turbidites (MIDDLETON, 1993), which are relevant to the oil industry. These deposits may be associated with density currents, whose movement occurs due to the density difference between the flow and the surrounding fluid (MIDDLETON, 1966; SIMPSON, 1997).

Mechanisms that govern the generation and migration of bedforms by density currents in marine environments are poorly understood because of the difficulty of direct observation, the limited number of experimental studies, and the complexity of these flows in relation to the fluvial (FEDELE; GUENTZEL; HOYAL, 2009). Consequently, some studies (PARKER et al., 1987; RAUDKIVI, 1997; PUHL, 2012; CARTIGNY; POSTMA, 2016, among many others) merge or even adapt existing knowledge about bedforms generated by fluvial flows assuming similar emergence and development between the two.

Some small scale experiments already performed with saline density currents or composed of suspended sediments (turbidity currents) analyzed the morphology of the mobile bed for different flow regimes (subcritical, critical, and supercritical). In general, lower plane beds, ripples, and dunes occur in subcritical flows (KNELLER; BENNETT; MCCAFFREY, 1997), whereas upper plane beds and antidunes are formed spontaneously in moving beds after supercritical flows (HAND, 1974; WINTERWERP et al., 1992; SPINEWINE et al., 2009; FEDELE; HOYAL; DRAPER, 2011).

Furthermore, Fedele, Guentzel and Hoyal (2009) identified a new type of bedform generated by density currents whose genesis resembles antidunes and whose development is similar to lower water-depth wavelength antidunes with migration in the flow

direction (unlike what usually occurs in free surface flows), due to the interaction at the interface between the shape and the flow.

In general, the prediction of bedforms by density currents is made based on stability diagrams (RAUDKIVI, 1990; CHANG, 1988) developed for fluvial bedforms despite differences between the hydraulic and sedimentological processes present in each case.

Among the several existing diagrams, this study analyzed the following four: Simons and Richardson (1961), Southard and Boguchwal (1990), Athallah (1968 apud JULIEN, 1998), and Van den Berg and Van Gelder (1993).

Simons and Richardson (1961) were the pioneers in the attempt to predict the types of bedforms, seeking to relate data from average grain size ( $d_{50}$ ) with flow's energy ( $\tau U$ ), establishing zones of probable occurrence of plane bed (lower and upper), ripples, dunes, and antidunes. Southard and Boguchwal (1990) developed one of the most used diagrams to predict bedforms, simple use and interpretation, which involves the direct plot of the average stream velocity and the average sediment size present in the bed.

Athallah's diagram (1968 apud JULIEN, 1998) correlates the dimensionless Froude number ( $Fr$ ) and the ratio between hydraulic radius ( $R_h$ ) and average grain size ( $d_{50}$ ), separating bedforms into zones of subcritical, critical, and supercritical flow regimes. Van den Berg and Van Gelder diagram (VAN DEN BERG; VAN GELDER, 1993) compares the dimensionless mobility parameter ( $\theta'$ ) and the average dimensionless grain size parameter ( $d_{50}^*$ ). The importance of the use of dimensionless parameters is emphasized by the last two authors, in the comparison of results among studies so that the scale effects present in the phenomenon be considered.

In view of the above, the present study applied an experimental methodology to generate bedforms by density currents and related the obtained results with the three mentioned fluvial phase diagrams in order to verify the applicability of these diagrams to the bedforms generated by density currents.

## METHODOLOGY

### Apparatus and experimental description

Experiments were performed in an 18 m long acrylic flume and rectangular cross section of 0.2 m x 0.5 m with a variable slope (Figure 1), built into a long masonry tank (25 m long and 0.74 x 1 m cross section).

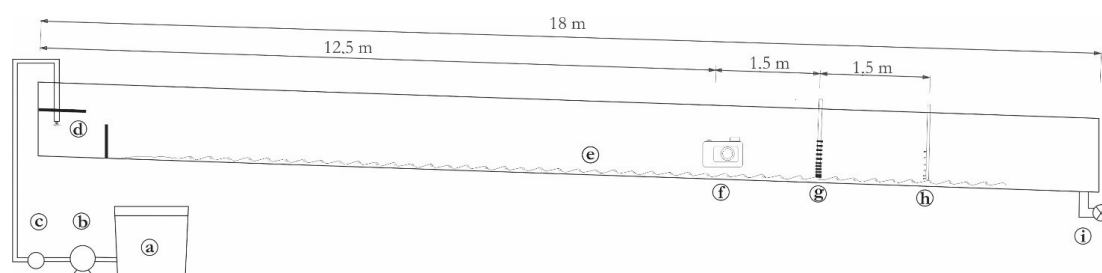


**Figure 1.** Test configuration (a) Reservoir for mixture preparation (b) Pump (c) Flow meter (d) Density current input (e) Mobile bed (f) Side views (g) UVP (h) Siphons and (i) Output valve.

Prior to each test, the bottom of the acrylic flume was filled with the sediment chosen to compose the mobile bed. Tests were performed in three types of beds identified as beach sand, river sand, and melamine, with density ( $\rho_s$ ) and characteristic grain sizes ( $d_{10}$ ,  $d_{50}$ ,  $d_{90}$ , and  $d_{50}^*$ ), which are shown in Table 1 and Figure 2. The dimensionless median grain sizes ( $d_{50}^*$ ) were calculated by Equation 1.

$$d_{50}^* = \left[ \frac{\left( \frac{\rho_s}{\rho_{amb}} - 1 \right) g d_{50}^3}{\nu^2} \right]^{1/3} \quad (1)$$

where  $\rho_{amb}$  is the water density (considered as  $998.2 \text{ kg m}^{-3}$ ),  $\rho_s$  is the density of the bed sediment ( $\text{kg m}^{-3}$ ),  $g$  is the gravitational acceleration ( $\text{m s}^{-2}$ ),  $d_{50}$  is the average grain size (m), and  $\nu$  is the kinematic viscosity ( $\text{m}^2 \text{ s}^{-1}$ ).

Regarding the morphoscopic properties, both sands were sub-rounded and with sphericity degree between moderate and high. In turn, melamine showed angular roundness and low sphericity (KRUMBEIN, 1963).

After some tests, a good part of the finer fraction of melamine had been transported to the output region of the acrylic flume. For this reason, a new sampling and particle size analysis of the melamine was performed, resulting in an average grain size of  $d_{50}$ :  $310 \text{ }\mu\text{m}$  (named melamine 2).

Grains of the three types of material used in the mobile bed were classified according to Folk and Ward (1957) as moderately selected, with selection degrees ( $\sigma$  ( $\Phi$ )) (Equations 2 and 3) between 0.53 and 0.73.

$$\sigma(\Phi) : \left( \frac{\%84 - \%16}{4} \right) \times \left( \frac{\%95 - \%5}{6,6} \right) \quad (2)$$

being,

$$\Phi : -\log_2(d) \quad (3)$$

where  $\sigma(\Phi)$  is the degree of sediment selection in relation to the  $\Phi$  parameter ( $\Phi$ ),  $\Phi$  is the scaling parameter, % 84 is the 84th percentile of the sample, % 16 is the 16th percentile of the sample, % 95 is the 95th percentile of the sample, % 5 is the 5th percentile of the sample, and  $d$  is the particle size ( $\mu\text{m}$ ).

In all, 29 tests were performed using three types of bed material, two input discharges, three values of input mixture concentration, and two flume slopes. Tests were named according to parameters, starting with the slope values ( $0.5^\circ$  or  $1.5^\circ$ ), followed by the type of bed (melamine - M, beach sand - P, and river sand - F), flow (q - low flows and Q - high flows), and density (low - 1, medium - 2, and high - 3). Tests with numbering 4 at the

**Table 1.** Grain size data of sediments used as mobile bed.

Bed	$\rho$ ( $\text{kg m}^{-3}$ )	$d$ ( $\mu\text{m}$ )			
		$d_{10}$	$d_{50}$	$d_{90}$	$d_{50}^*$
Melamine	1500	165	245	410	3.9
Melamine 2	1500	169	310	487	4.9
Sand beach	2600	131	206	324	4.8
River sand	2600	208	480	790	11.3

end are related to repetitions performed with parameters similar to those of final 3.

The saline mixture was prepared in a reservoir of 5000 L capacity (Figure 1a), with density values of 1015, 1025, and  $1040 \text{ kg m}^{-3}$  and respective salt concentrations of 26, 42, and  $67 \text{ g L}^{-1}$ . After the mixture homogenization, its temperature was measured with a thermometer and its density through a hydrometer. After leveling of the mobile bed, the approximate thickness of 5 cm, and slow filling of the flume with water (besides recording the temperature and density considered equal to  $998.2 \text{ kg m}^{-3}$ ), the experiment was started. From the start of the pump (Figure 1b), the saline mixture was introduced into the experimental flume (Figure 1d), being its inflow recorded by the flow meter (Figure 1c) coupled to the pipe.

During the entire flow of the density current (Figure 3 - stained with a red dye for better visualization), the average velocity (Figure 1g - Ultrasound Velocity Profile - Duo MetFlow AS) and concentration profiles (Figure 1h - siphons and refractometer) were recorded throughout the experiment. Velocity profiles were composed of ten sensors (Figure 4a) disposed at 0.08, 2.15, 4.95, 7.9, 10.8, 13.7, 18, 22.4, 26.7, and 31.1 cm from the mobile bed and positioned at 14 m of the saline stream injection, with an acquisition frequency of 2 Hz. Profiles of average values of concentration (Figure 4b) were constructed from samples collected in 3.5 and 6 mm siphons of internal and external diameter, respectively, located at 2, 5, 10, 13, 18, and 21 cm of

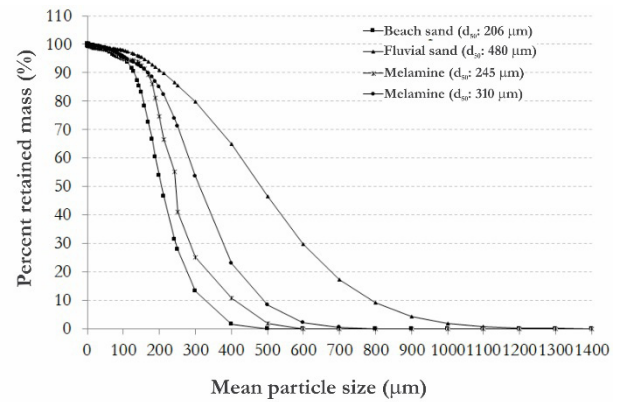


**Figure 2.** Grain size distribution of sediments used in mobile beds.

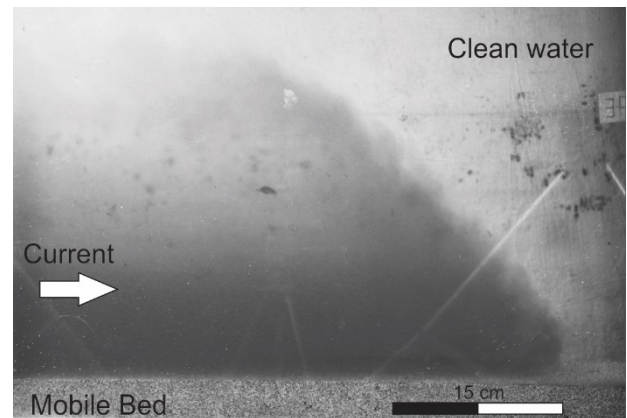


**Figure 3.** Density current performed in experiment 0.5Mq1\* (Q:  $380 \text{ L min}^{-1}$ ,  $\rho_{CD}$ :  $1016 \text{ kg m}^{-3}$ ,  $C_{CD}$ :  $11.3 \text{ g L}^{-1}$ ).

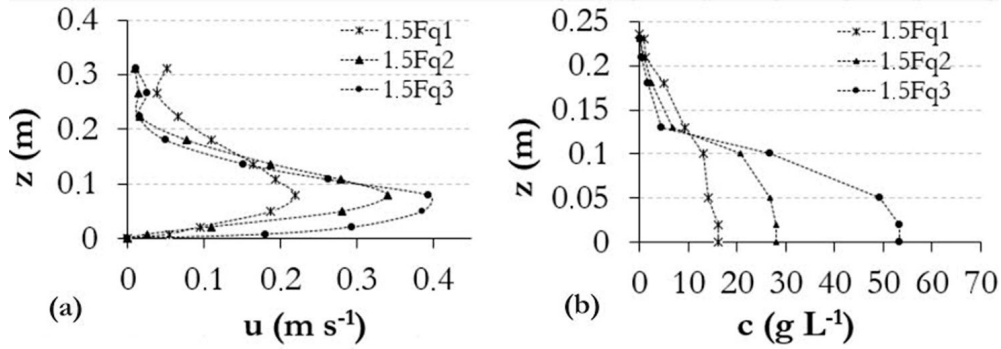


**Figure 4.** Velocity (a) and concentration (b) profiles of density currents from experiments 1.5Fq1 ( $U = 0.15 \text{ m s}^{-1}$  and  $C_{CD} = 9.0 \text{ g L}^{-1}$ ), 1.5Fq2 ( $U = 0.24 \text{ m s}^{-1}$  and  $C_{CD} = 16.3 \text{ g L}^{-1}$ ) and 1.5Fq3 ( $U = 0.29 \text{ m s}^{-1}$  and  $C_{CD} = 30.6 \text{ g L}^{-1}$ ).

the mobile bed and 15.5 m of the saline stream. Seven samples were taken throughout the test, whose densities were read by a portable refractometer ATAGO S28E 2 ~ 28% and converted to salt concentration from a calibration curve performed in laboratory (Equation 4)

$$\rho = 0.643C + 998.2 \quad (4)$$

where  $\rho$  is the saline density read by the refractometer ( $\text{kg m}^{-3}$ ) and  $C$  is the salt concentration ( $\text{g L}^{-1}$ ).

Furthermore, the analysis of the generation and development of bedforms as well as the current thickness was performed every second based on pictures obtained laterally to the flume, using a Nikon D5000 camera (Figure 1f) as described by Koller (2016).

The output valve (sphere) located at the end of the masonry flume (near its bottom and after 3 m of the end of acrylic flume) was opened in order to keep the water level of the long tank (Figure 1i) shortly after the beginning of the experiment.

Finally, after pumping an average of 4000 L of the mixture per test (for about 8 min), the tank was slowly emptied in order to not disturb any bedforms generated by the density current.

After the full drainage of the long tank, pictures were taken from the top along the whole acrylic flume.

## Data analysis

During the flow of density currents, characteristic velocity profiles ( $u$ ) and concentration ( $c$ ) are developed, whose vertical values vary according to the distance in relation to the bed ( $z$ ) and over time ( $t$ ).

The calculation of average values of velocity ( $U$ ), concentration ( $C_{CD}$ ), and thickness ( $H$ ) of density currents in the flow direction was performed by summation of adapted Ellison and Turner (1959) in Equations 5, 6, and 7.

$$UH = \int_0^{\infty} u dz = \sum_{i=1}^{m-1} \frac{u_i + u_{i+1}}{2} (z_{i+1} - z_i) \quad (5)$$

$$U^2 H = \int_0^{\infty} u^2 dz = \sum_{i=1}^{m-1} \frac{u_i^2 + u_{i+1}^2}{2} (z_{i+1} - z_i) \quad (6)$$

$$UC_{DC}H = \int_0^{\infty} u c dz = \sum_{i=1}^{m-1} \frac{u_i c_i + u_{i+1} c_{i+1}}{2} (z_{i+1} - z_i) \quad (7)$$

where  $U$  is the mean velocity of the density current ( $\text{m s}^{-1}$ ),  $u$  is the current velocity in the flow direction ( $\text{m s}^{-1}$ ),  $H$  is the mean current thickness ( $\text{m}$ ),  $z$  is the vertical distance to the bed ( $\text{m}$ ),  $C_{DC}$  is the mean current concentration ( $\text{g L}^{-1}$ ), and  $c$  is the current concentration at the sampling point ( $\text{g L}^{-1}$ ).

Near-bed shear velocities ( $u^*$ ) were estimated based on velocity data collected near the mobile bed-current density interface, in the region below the maximum current velocities. This region of the velocity profile presented a logarithmic distribution for all tests of the present work and, therefore, the shear velocity calculation of the flow was performed according to Equation 8 as already applied for current density, according to Altinakar, Graf and Hopfinger (1996) and Manica (2009).

$$\frac{u}{u^*} = \frac{1}{\kappa} \ln \left( \frac{z}{z_0} \right) \quad (8)$$

where  $u$  is the current velocity in flow direction ( $\text{m s}^{-1}$ ),  $z$  is the distance to the bed ( $\text{m}$ ),  $z_0$  is the distance to the point where the velocity reaches zero ( $\text{m}$ ),  $u^*$  is the shear velocity ( $\text{m s}^{-1}$ ), and  $\kappa$  is the von Kármán constant (0.41).

The shear velocity represents an intensity measure of the turbulent fluctuations (GRAF, 1971) and is used on the shear stress calculation of the flow near the bed ( $\tau_b$ ) which, in turn, is an input parameter in phase diagrams from Simons and Richardson (1961). Such calculation was based on Equation 9 adapted from fluvial flows (YALIN, 1972), replacing the density of fluvial flow by density currents ( $\rho_{DC}$ ), neglecting any stresses from the fluid.

$$u^* = \sqrt{\frac{\tau_b}{\rho_{DC}}} \quad (9)$$

where  $u^*$  is the shear velocity ( $\text{m s}^{-1}$ ),  $\tau_b$  is the shear stress near the bed ( $\text{N m}^{-2}$ ), and  $\rho_{DC}$  is the density of the density current ( $\text{kg m}^{-3}$ ).

Finally, the calculation of the grain mobility parameter ( $\theta$ ) and the dimensionless median grain size ( $d_{50}^*$ ) used as input parameters of the Van den Berg and Van Gelder diagram (VAN DEN BERG; VAN GELDER, 1993) are presented in Equations 10 and 11.

$$\theta' = \frac{\rho_{DC} U^2}{(\rho_s - \rho_{DC}) C'^2 d_{50}} \quad (10)$$

being,

$$C' = 18 \log \left( \frac{4H}{d_{90}} \right) \quad (11)$$

where,  $\theta'$  is the grain mobility parameter,  $\rho_{DC}$  is the density of the density current ( $\text{kg m}^{-3}$ ),  $\rho_s$  is the density of the bed sediment ( $\text{kg m}^{-3}$ ),  $U$  is the current mean velocity ( $\text{m s}^{-1}$ ),  $H$  is the current mean thickness (m),  $C'$  is the Chézy's coefficient,  $d_{50}$  is the mean grain size (m),  $d_{90}$  is the characteristic grain size, in which 90% of particles show smaller sizes (m) and  $d_{30}$  is the median grain size (m).

The relation between the inertial and gravitational forces of density currents defined by the dimensionless densimetric Froude ( $Fr_d$ ) classifies it in subcritical ( $Fr_d < 1$ ), critical ( $Fr_d = 1$ ), and supercritical ( $Fr_d > 1$ ) regimes, as shown in Equation 12.

$$Fr_d = \frac{U}{\sqrt{\frac{\rho_{DC} - \rho_{amb}}{\rho_{amb}} gH}} \quad (12)$$

where  $U$  is the average velocity of the density current ( $\text{m s}^{-1}$ ),  $\rho_{DC}$  is the density of the density current ( $\text{kg m}^{-3}$ ),  $\rho_{amb}$  is the density of the ambient water ( $\text{kg m}^{-3}$ ),  $g$  is the gravitational acceleration ( $\text{m s}^{-2}$ ), and  $H$  is the current mean thickness (m).

The parameter presented above, together with the dimensionless relationship between the hydraulic radius ( $R_h$ ) and  $d_{50}$  (defined by the author as relative submergence) presented in Equation 13 are used in the Athallah's phase diagram (1968 apud JULIEN, 1998).

$$R_h = \frac{A}{p} = \frac{lh}{1+2h} \quad (13)$$

where  $l$  and  $h$  are considered the width and the thickness of the flow, respectively. For the calculation of this parameter, the present study considered the stream average height and the width of the two-dimensional flume.

Besides parameters related to currents and mobile beds used in the diagram analysis, it was also necessary to know the types of generated bedforms. Thus, the bedforms were classified with regard to two factors: (a) sediment transport near the bed and the presence of suspended sediments during its generation, verified by images obtained during the tests and (b) the size of bedforms.

## RESULTS

### Density current

The average values of velocity and concentration of density currents obtained from their respective profiles and using Equations 5 and 6 are presented in Table 2.

All velocity and concentration profiles follow classic trends for density currents as stated by other authors (FABIAN, 2002; MANICA, 2009; SEQUEIROS, 2012; PUHL, 2012). Figure 4 shows velocity (Figure 4a) and concentration

profiles of density currents (Figure 4b) which were analyzed in the present study.

Velocity values are reduced near the bed due to the interaction between the flow and the mobile bed and then increase up to a maximum point (positive velocity gradient), defining the lower boundary layer of the profile similar to a turbulent boundary layer (YALIN, 1972).

As can be seen in Figure 4, this region was characterized by four sampling points (considering  $u^*$  null at rate 0). Based on these values and the use of Equation 8, the shear velocity of the flow near the bed ( $u^*$ ) could be calculated (Table 3). Above the maximum velocity value, they keep decreasing until reach the upper stream layer (mixture layer), where there is greater incorporation of the ambient water present in the long tank and consequent decrease of concentration of the density current.

However, concentration profiles (Figure 4b) presented higher values near the bed, attenuating along the vertical until reach the interface with the ambient water, where there is a greater incorporation of the ambient water.

Shear stresses ( $\tau_b$ ), fundamental in the definition of forces exerted by the flow and used in the calculation of the mobility parameter of the Simons and Richardson diagram (SIMONS; RICHARDSON, 1961), were calculated from Equations 8 and 9 and are presented in table 3.

Shear velocities ( $u_s$ ) for all the tests ranged from 0.08 to 2.51  $\text{m s}^{-1}$  and the shear stress ( $\tau_b$ ) between 0.18 and 3.25  $\text{N m}^{-2}$ .

Table 4 shows mobility parameters ( $\theta'$ ) calculated from Equations 10 and 11 with values ranging from 0.01 to 0.33.

The maximum values of  $\theta'$  occur for beds composed of melamine and for high discharge flows, concentrations and flume slopes, indicating the high mobility of this sediment for the referred hydraulic conditions.

On the other hand, the lower values of  $\theta'$  resulting from experiments performed on river sand (of greater diameter and density than melamine), pointing to this sediment as the most difficult to be mobilized.

The densimetric Froude number contemplated a considerable range of values (between 0.5 and 2.2) (Table 5), occurring 8 experiments with flow of subcritical regime and 21 in the supercritical regime, as shown in Table 5.

In general, density currents with low  $Fr_d$  values have developed plane beds and smaller bedforms, such as ripples. Inasmuch as  $Fr_d$  increased, bedforms also increased in size (length and height), tending to generate dunes and/or supercritical plane beds.

### Bedforms

Based on the lateral images obtained during the tests together with the calculated shear stress values, it was possible to classify the bedforms generated in lower plane bed, ripples, and dunes (Figure 5).

The lower plane bed occurred with high frequency, 12 out of 29 tests. During the tests that generated plane bedforms, no suspension or movement of the grains was noticed near the bed.

**Table 2.** Discharge (Q), velocity (U), thickness (H) and concentrations of mixture ( $C_0$ ) and density current ( $C_{DC}$ ).

Test	Q (L min <sup>-1</sup> )	U (m s <sup>-1</sup> )	$C_0$ (g L <sup>-1</sup> )	$C_{DC}$ (g L <sup>-1</sup> )	H (m)
0.5Mq1*	380	0.14	26.9	11.3	0.26
0.5Mq2*	384	0.15	43.3	17.6	0.23
0.5Mq3	383	0.18	68.2	40.7	0.23
0.5MQ1*	506	0.20	27.7	12.7	0.20
0.5MQ2	517	0.20	51.1	30.8	0.25
0.5MQ3	479	0.19	63.5	27.1	0.25
0.5MQ4	474	0.13	72.8	41.5	0.25
1.5Mq1	382	0.10	27.7	10.9	0.24
1.5Mq2	383	0.22	39.4	18.0	0.20
1.5Mq3	383	0.28	65.8	32.7	0.19
1.5MQ1	517	0.21	27.7	11.1	0.25
1.5MQ2	520	0.26	41.7	20.8	0.23
1.5MQ3	519	0.36	69.7	45.8	0.19
0.5PQ1	504	0.13	18.4	6.4	0.29
0.5PQ2	503	0.20	40.2	25.3	0.29
0.5PQ3	506	0.26	66.6	39.3	0.24
1.5Pq1	364	0.16	26.1	7.3	0.20
1.5Pq2	364	0.21	43.6	16.4	0.17
1.5Pq3	383	0.25	72.8	30.9	0.14
1.5Pq4	326	0.25	66.9	29.7	0.16
1.5PQ1	509	0.23	26.3	8.3	0.20
1.5PQ2	516	0.25	41.7	15.0	0.23
1.5PQ3	461	0.30	68.2	35.1	0.17
0.5FQ1	508	0.16	26.9	10.2	0.27
0.5FQ2	504	0.20	41.7	16.2	0.25
0.5FQ3	508	0.25	66.6	41.5	0.25
1.5Fq1	381	0.15	26.9	9.0	0.24
1.5Fq2	380	0.24	42.5	16.3	0.17
1.5Fq3	379	0.29	66.1	30.6	0.16
1.5Fq4	377	0.28	66.0	27.9	0.16

\* Experiments performed with the “melamine 2” sediment.

**Table 3.** Calculated velocity  $u^*$  and shear ( $\tau_b$ ) stresses.

Test	$u^*$ (m s <sup>-1</sup> )	$\tau_b$ (N m <sup>-2</sup> )	Test	$u^*$ (m s <sup>-1</sup> )	$\tau_b$ (N m <sup>-2</sup> )
0.5Mq1*	0.14	0.21	0.5PQ3	0.49	1.60
0.5Mq2*	0.29	0.44	1.5Pq1	0.08	0.26
0.5Mq3	0.61	0.69	1.5Pq2	0.32	1.06
0.5MQ1*	1.13	1.70	1.5Pq3	0.20	0.66
0.5MQ2	0.22	0.25	1.5Pq4	0.22	0.73
0.5MQ3	0.37	0.43	1.5PQ1	0.50	1.66
0.5MQ4	0.28	0.32	1.5PQ2	0.23	0.78
1.5Mq1	0.15	0.18	1.5PQ3	0.44	1.46
1.5Mq2	0.92	1.08	0.5FQ1	0.22	1.69
1.5Mq3	2.51	2.90	0.5FQ2	0.09	0.71
1.5MQ1	0.42	0.49	0.5FQ3	0.10	0.74
1.5MQ2	1.27	1.50	1.5Fq1	0.11	0.88
1.5MQ3	1.43	1.62	1.5Fq2	0.42	3.25
0.5PQ1	0.10	0.32	1.5Fq3	0.28	2.18
0.5PQ2	0.19	0.64	1.5Fq4	0.33	2.55

\* Experiments performed with the “melamine 2” sediment.

The beginning of ripples generation occurred in a slow way, where the interaction between the flow and the bed did not allow the suspension of large amounts of sediment, perceptible by the image analyses. These bedforms presented mild upstream slopes and more abrupt downstream slopes occurring in 13 of the 29 experiments.

Dunes were identified in four tests within 29 performed (1.5Mq2, 1.5Mq3, 1.5MQ2, and 1.5MQ3). These bedforms differ from ripples due to the high shear stress applied by the flow near the bed ( $1.08 < \tau_b$  (N m<sup>-2</sup>) < 2.90) and by the visible transport of sedimentary material next to the bed and in suspension.

**Table 4.** Chézy's coefficient values ( $C'$ ) and the mobility parameter ( $\theta'$ ).

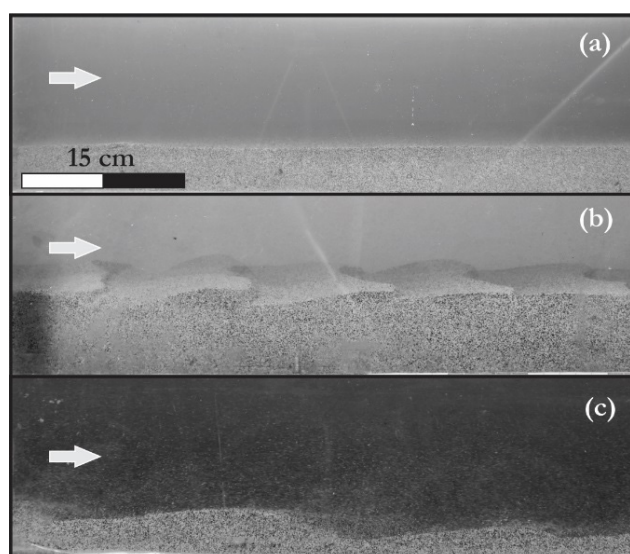
Test	$C'$	$\theta'$	Test	$C'$	$\theta'$
0.5Mq1*	60.0	0.04	0.5PQ3	62.6	0.05
0.5Mq2*	60.3	0.04	1.5Pq1	60.9	0.02
0.5Mq3	60.2	0.08	1.5Pq2	59.7	0.04
0.5MQ1*	58.0	0.08	1.5Pq3	58.2	0.06
0.5MQ2	61.0	0.09	1.5Pq4	59.1	0.05
0.5MQ3	60.8	0.08	1.5PQ1	61.2	0.04
0.5MQ4	60.9	0.04	1.5PQ2	62.0	0.05
1.5Mq1	60.5	0.02	1.5PQ3	59.7	0.08
1.5Mq2	59.1	0.11	0.5FQ1	56.3	0.01
1.5Mq3	58.7	0.20	0.5FQ2	56.1	0.02
1.5MQ1	61.1	0.10	0.5FQ3	55.7	0.03
1.5MQ2	60.4	0.16	1.5Fq1	55.4	0.01
1.5MQ3	58.9	0.33	1.5Fq2	52.6	0.03
0.5PqQ1	63.9	0.01	1.5Fq3	52.4	0.04
0.5PQ2	63.8	0.03	1.5Fq4	52.4	0.04

\* Experiments performed with the "melamine 2" sediment.

**Table 5.** Values of densimetric Froude number ( $Fr_d$ ) of the experimentally generated density currents.

Test	$Fr_d$	Test	$Fr_d$	Test	$Fr_d$
0.5Mq1*	1.02	1.5MQ1	1.59	1.5PQ1	2.18
0.5Mq2*	0.92	1.5MQ2	1.50	1.5PQ2	1.70
0.5Mq3	0.79	1.5MQ3	1.53	1.5PQ3	1.56
0.5MQ1*	1.55	0.5PqQ1	1.20	0.5FQ1	1.22
0.5MQ2	0.91	0.5PQ2	0.93	0.5FQ2	1.23
0.5MQ3	0.91	0.5PQ3	1.04	0.5FQ3	0.97
0.5MQ4	0.51	1.5Pq1	1.71	1.5Fq1	1.32
1.5Mq1	0.81	1.5Pq2	1.62	1.5Fq2	1.84
1.5Mq2	1.45	1.5Pq3	1.54	1.5Fq3	1.66
1.5Mq3	1.35	1.5Pq4	1.44	1.5Fq4	1.64

\* Experiments performed with the "melamine 2" sediment.

**Figure 5.** Bedforms generated. (a) lower plane bed, (b) ripples, and (c) dunes.

## Phase diagrams

Based on presented hydraulic parameters together with types of generated bedforms, the input parameters of phase diagrams were calculated and are presented below.

### Simons and Richardson (1961)

This phase diagram was a pioneer in the attempt to predict the bedform types, seeking to relate data from average grain size ( $d_{50}$ ) with flow's energy ( $U\tau$ ). Figure 6 shows these parameters for tested density currents in the Simons and Richardson diagram, indicating the incidence of most points in the prediction region of ripples.

Only three points were found in the dune prediction referring to 1.5Fq2, 1.5Fq3, and 1.5Fq4 tests, conducted in sand-bed river ( $d_{50} = 480 \mu\text{m}$ ), whereas the last two showed ripples with high wavelengths.

Besides ripples, it can be observed the occurrence of dunes (1.5Mq2, 1.5Mq3, 1.5MQ2, and 1.5MQ3 - indicated by the

triangles) and seven lower plane beds (1.5Fq1, 0.5FQ3, 0.5FQ2, and 0.5FQ1 - river sand and 0.5Pq2, 0.5Pq3, and 1.5PQ1 - beach sand). Even in the ripple region, it is emphasized the proximity of the 1.5Mq3 experiment (with larger dimensions) with the self-prediction region showed coherence in the flow's energy and the average grain size required to generate this bedform.

Experiments whose points are located in the predicted region to form lower plane bed resulted in ripples (0.5Mq2, 0.5MQ3, 0.5MQ4, and 1.5Mq1) and lower plane beds (0.5Mq1\*, 0.5Mq2\*, 0.5Pq1, and 1.5Pq1). The occurrence of ripples in this region can be explained by the composition of the bed used in these tests (melamine), which has been shown to be an easier material to be remobilized due to its low density. Although melamine has a density of  $1500 \text{ kg m}^{-3}$  (plastic material), the sand has approximately  $2650 \text{ kg m}^{-3}$  due to its quartz composition.

Finally, the diagram showed good predictions for ripples generated in beds composed of beach sand, similar sediment to that used by the diagram's author.

**Southard and Boguchwal (1990)**

Average velocities of density currents, together with the average grain size of the tested bedforms in the Southard and Boguchwal diagram (SOUTHARD; BOGUCHWAL, 1990) are shown in Figure 7.

Although the present study identified three distinct bedforms (lower plane bed, ripples, and dunes), these authors predicted only the generation of ripples based on average velocities of density currents and the average grain size of the used bedforms.

As a hypothesis of differences between the observed bedforms and those predicted by the diagram, the bedform from velocity profiles of the fluvial flows (from which the diagram was elaborated) is emphasized, which is different from density currents. This might have influenced both the calculated average stream velocity (y-axis of the diagram) and the velocity near the bed. Furthermore, the average grain size (parameter used on the x-axis of the diagram) does not consider the density of the material present in the bed, which impairs its comparison with studies performed with different sediments.

Additionally, the cited differences relate to test conditions used by the author, who established average flow thicknesses between 0.25 and 0.40 m and used only sand as mobile bed material.

**Athallah (1968 apud JULIEN, 1998)**

This author constructed a classification diagram for bedforms, considering the flow regime (subcritical, critical, and supercritical) by calculating the dimensionless Froude numbers ( $Fr$ ) and by the relationship between the hydraulic radius ( $R_h$ ) and the average grain size ( $d_{50}$ ) - defined as relative submergence.

Although Froude number defined flow regimes through their values (smaller, equal or greater than unity), Athallah (1968 apud JULIEN, 1998) constructed his diagram defining these regimes based on the occurrence of ripples and dunes (Supercritical regime), plane bed transition (critical regime), and antidunes, falls, and pools (supercritical regime). The uncertainty associated with the direct use of the Froude number for the prediction of bedforms is emphasized by the authors.

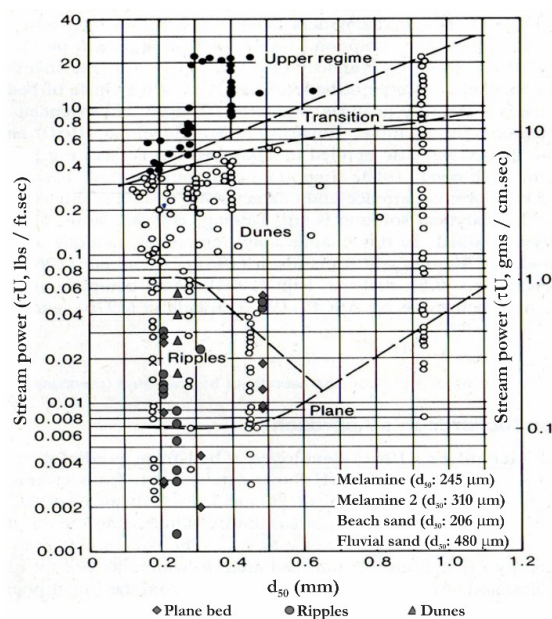


**Figure 6.** Experimental results applied to the Simons and Richardson diagram (SIMONS; RICHARDSON, 1961).

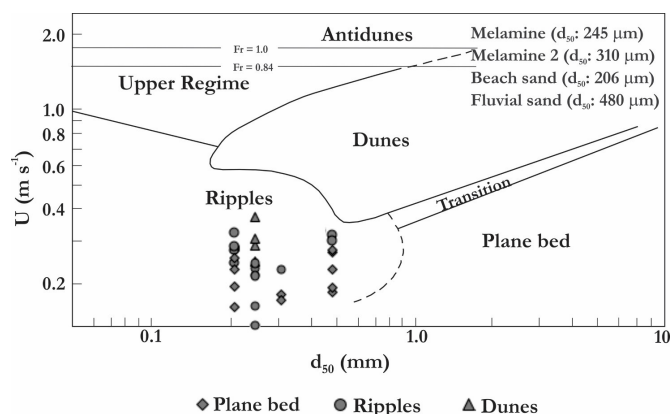


**Figure 7.** Experimental results plotted in the Southard and Boguchwal diagram (SOUTHARD; BOGUCHWAL, 1990).

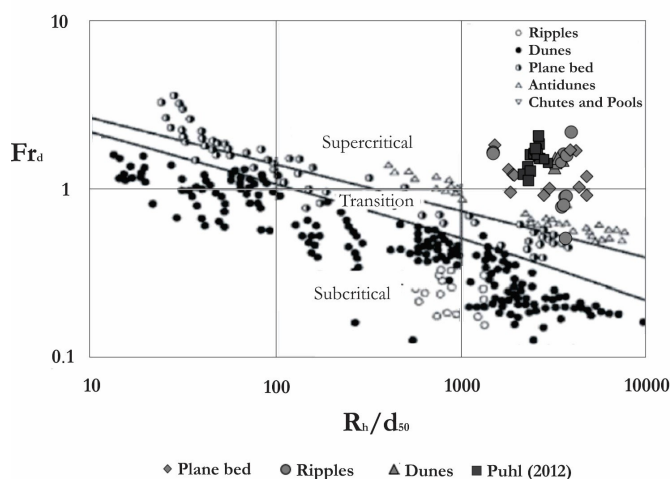


**Figure 8.** Athallah's diagram (1968 apud JULIEN, 1998) with the application of parameters of densimetric Froude ( $Fr_d$  - adapted from  $Fr$ ) and relative submergence ( $R_h/d_{50}$ )

In the present study, the use of this diagram was adapted by calculating the densimetric Froude number ( $Fr_d$ ), which considers the small density difference between the current and the ambient fluid in the thrust force.

Figure 8 shows  $Fr_d$  values and relative submergence ( $R_h/d_{50}$ ) calculated for the experimental current densities. It was identified the simultaneous occurrence of the three types of generated bedforms (plane bed, ripples, and dunes) in a region defined by approximate values of  $Fr_d=1.5$  and  $R_h/d_{50}=3000$ . In other words, with the exception of the test 0.5MQ4 ( $Q=474\text{ L min}^{-1}$ ,  $U=0.13\text{ ms}^{-1}$ , and  $Fr_d=0.5$ ), all plotted points were restricted to the region of the predicted flow chart of supercritical regime (even with  $Fr_d$  smaller than 1) and of antidunes' formation. However, none of the bedforms generated by density currents showed antidune characteristics (very symmetrical forms, larger dimensions in relation to the dunes, and flow surface in phase with bedforms, according to Simon and Richardson (1961) and Engelund and Fredsøe (1982)).

Furthermore, there are plane beds and ripples mapped in regions with high  $Fr_d$ , however, these forms were not predicted for supercritical fluvial flow regimes.

Although they differ from results found by Athallah, the values of the present study approximate those found by Puhl (2012), showing consistency among the observations of bedforms by density currents.

Finally, the dimensionlessness of results in the mentioned parameters does not show any evident trend for grouping on the regions in the diagram, precluding its use for the prediction of bedforms by density currents. The use of  $Fr_d$  might have influenced this result, since the density difference between the current and the ambient fluid must be considered in this calculation (differently from the  $Fr$  number).

The wide use of the Froude number ( $Fr$ ) in the classification of bedforms generated by fluvial flow is highlighted. However, several studies (FEDELE; GUENTZEL; HOYAL, 2009; PUHL, 2012; CARTIGNY; POSTMA, 2016) show the need for adapting the prediction of bedforms generated by density currents based on  $Fr_d$ , since the profiles of velocity and concentration and hence the hydraulic processes present in these flows differ from those to the free surface.

### Van den Berg and Van Gelder (1993)

This diagram is a review of Van Rijn's diagram (VAN RIJN, 1984), which considers the influence of shear stresses on the occurrence and dimensions of bedforms as a basic element of this approach and relates the average dimensionless grain size ( $d_{50}^*$ ) with the mobility parameter ( $\theta^*$ ).

Figure 9 shows the application of these parameters to the tested density currents and to the used bedforms.

All experiments that generated ripples (indicated by circles) are located in the region predicted for this type of bedform regardless of the type and average grain size of sediment used in the mobile bed (melamine or sand).

Among the four experiments classified as dunes, only 1.5MQ3 is located in the prediction region for these bedforms due to the influence of its high velocity in the calculation of mobility parameter. The other three experiments (1.5MQ2, 1.5MQ3, and 1.5MQ2),

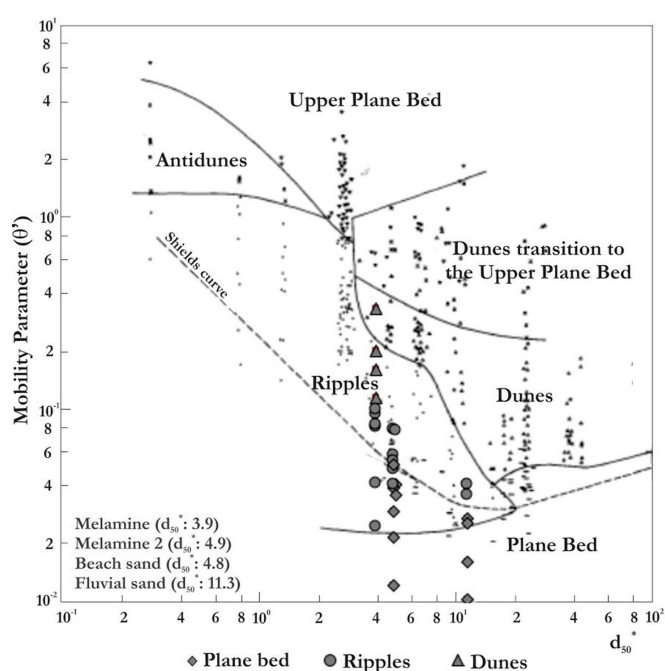


**Figure 9.** Prediction diagram of Van den Berg and Van Gelder (1993) from data obtained experimentally in this study.

although located in the prediction region of ripples, are close to the region established for dunes, according to the author.

It should be noted that the lower region of the diagram predicts the occurrence of lower plane bed, where four from the twelve experiments showed this configuration. Although the rest of the generated lower plane beds (indicated by diamonds) have been located in the prediction region of ripples, they are still below the Shields curve (region of absence of particle movement, according to Shields (1936)).

Thus, the results obtained in the present study seem to correspond well with those predicted by Van den Berg and Van Gelder diagram (VAN DEN BERG; VAN GELDER, 1993). This is because these authors have correlated dimensionless parameters in their prediction, allowing the comparison of results obtained with different scales and sediment compositions.

## CONCLUSIONS

The present study generated three types of bedforms (lower plane bed, ripples, and dunes) through experiments with density currents, on a reduced scale. The parameters' analysis of these currents and sediments used in the composition of the mobile beds made it possible to calculate the input parameters of three types of prediction diagram of fluvial bedforms besides the verification of their application and validity in the prediction of bedforms by density currents.

Results showed that bedforms generated by density currents presented disagreements in relation to those predicted by the discussed fluvial stability diagrams. Regarding dimensionless diagrams of Simons and Richardson (1961) and Southard and Boguchwal (1990), this disagreement may have been influenced by the difference between the materials (size, density, shape) used in the present study in relation to those used in the cited diagrams.

Athallah's diagram (1968 apud JULIEN, 1998) despite using dimensionless parameters in its analysis, clearly did not show a good correlation with observations of fluvial flows neither grouped the different bedforms. However, Van den Berg and Van Gelder (1993) grouped the data in different regions, although they did not respect the prediction limits of fluvial bedforms.

The hydraulic differences between the fluvial flows (free surface) when compared to the density currents (two different interfaces and different velocity and concentration profiles) are highlighted as the main source of the differences between the experimental results of this study and the presented phase diagrams

Thereby, it is evident the need for specific studies that help in the elaboration of a proper diagram for the prediction of bedforms generated by density currents. Such a diagram can only be obtained from observations under experimentally controlled conditions, through safety in the correlation of hydrodynamic and sedimentological data.

## ACKNOWLEDGEMENTS

The first author acknowledges CNPq (National Council for Scientific and Technological Development) and, together with the other authors, to the ExxonMobil Upstream Research Company.

## REFERENCES

ALTINAKAR, M. S.; GRAF, W. H.; HOPFINGER, E. J. Flow structure in turbidity currents. *Journal of Hydraulic Research*, v. 34, n. 5, p. 713-718, 1996. <http://dx.doi.org/10.1080/00221689609498467>.

CARTIGNY, M. J. B.; POSTMA, G. Turbidity current bedforms. In: GUILLEN, J.; ACOSTA, J.; CHIOCCI, F. L.; PALANQUES, A. *Atlas of bedforms in the Western Mediterranean*. New York: Springer, 2016. p. 29-33.

CHANG, H. H. *Fluvial processes in river engineering*. New York: John Wiley, 1988. p. 432.

ELLISON, T. H.; TURNER, J. S. Turbulent entrainment in stratified flows. *Journal of Fluid Mechanics*, v. 6, n. 3, p. 423-448, 1959. <http://dx.doi.org/10.1017/S0022112059000738>.

ENGELUND, F.; FREDSE, J. Sediment ripples and Dunes. *Annual Review of Fluid Mechanics*, v. 14, n. 1, p. 13-37, 1982. <http://dx.doi.org/10.1146/annurev.fl.14.010182.000305>.

FABIAN, S. *Modelagem física de correntes de densidade conservativas em canal de declividade variável*. 2002. 107 f. Dissertação (Mestrado em Engenharia) - Instituto de Pesquisas Hidráulicas. Programa de Pós-Graduação em Engenharia de Recursos Hídricos e Saneamento Ambiental, Universidade Federal do Rio Grande do Sul, Porto Alegre, 2002.

FEDELE, J. J.; GUENTZEL, K.; HOYAL, D. C. Experiments on bedforms created by density currents. In: RIVER, COASTAL AND ESTUARINE MORPHODYNAMICS SYMPOSIUM, 9., 2009, Boca Raton. *Proceedings...* Boca Raton: CRC Press, 2009. p. 833-840.

FEDELE, J. J.; HOYAL, D. C.; DRAPER, J. M. Supercritical bedforms under density currents. In: RIVER COASTAL AND ESTUARINE MORPHODYNAMICS – RCEM, 5., 2011, Beijing, China. *Proceedings...* Beijing: Regional Civil Society Engagement Mechanism, 2011. p. 1- 9.

FOLK, R. L.; WARD, W. C. Brazos River bar: a study in the significance of grain size parameters. *Journal of Sedimentary Petrology*, v. 27, n. 1, p. 3-26, 1957. <http://dx.doi.org/10.1306/74D70646-2B21-11D7-8648000102C1865D>.

GRAF, W. H. *Hydraulics of sediment transport*. New York: McGraw-Hill, 1971. 513 p. (Series in Water Resources and Environmental Engineering).

HAND, B. M. Supercritical flow in density currents. *Journal of Sedimentary Petrology*, v. 44, n. 3, p. 637-648, 1974.

JULIEN, P. Y. *Erosion and sedimentation*. Cambridge: Cambridge University Press, 1998.

KNELLER, B. C.; BENNETT, S. J.; MCCAFFREY, W. D. Velocity and turbulence structure of density currents and internal solitary waves: potential sediment transport and the formation of wave ripples in deep water. *Sedimentary Geology, Amsterdam*, v. 112, n. 3-4, p. 235-250, 1997. [http://dx.doi.org/10.1016/S0037-0738\(97\)00031-6](http://dx.doi.org/10.1016/S0037-0738(97)00031-6).

KOLLER, D. K. *Estudo experimental de formas de fundo por correntes de densidade salina em canal de fundo móvel*. 2016. 120 f. Dissertação (Mestrado em Recursos Hídricos e Saneamento Ambiental) - Instituto de Pesquisas Hidráulicas, Universidade Federal do Rio Grande do Sul, Porto Alegre, 2016.

KRUMBEIN, W. C. *Stratigraphy and sedimentation*. 2nd ed. San Francisco: Freeman, 1963. 660 p.

MANICA, R. *Geração de correntes de turbidez de alta densidade: condicionantes hidráulicos e deposicionais*. 2009. 391 f. Tese (Doutorado em Recursos Hídricos e Saneamento Ambiental) - Instituto de Pesquisas Hidráulicas, Universidade Federal do Rio Grande do Sul, Porto Alegre, 2009.

MIDDLETON, G. V. Experiments on density and turbidity currents I. Motion of the head. *Canadian Journal of Earth Sciences*, v. 3, n. 4, p. 523-546, 1966. <http://dx.doi.org/10.1139/e66-038>.

MIDDLETON, G. V. Sediment deposition from turbidity currents. *Annual Review of Earth Planet Science*, v. 21, p. 89-114, 1993.

PARKER, G.; GARCIA, M.; FUKUSHIMA, Y.; YU, W. Experiments on turbidity currents over an erodible bed. *Journal of Hydraulic Research*, v. 25, n. 1, p. 123-147, 1987. <http://dx.doi.org/10.1080/00221688709499292>.

PUHL, E. *Morfodinâmica e condição de equilíbrio do leito sob a ação de correntes de turbidez*. 2012. 155 f. Tese (Doutorado em Recursos Hídricos e Saneamento Ambiental) - Instituto de Pesquisas

- Hidráulicas, Universidade Federal do Rio Grande do Sul, Porto Alegre, 2012.
- RAUDKIVI, A. J. *Loose boundary hydraulics*. 3rd ed. Oxford: Pergamon Press, 1990. 538 p.
- RAUDKIVI, A. J. Ripples on stream bed. *Journal of Hydraulic Engineering*, v. 123, n. 1, p. 58-64, 1997. [http://dx.doi.org/10.1061/\(ASCE\)0733-9429\(1997\)123:1\(58\)](http://dx.doi.org/10.1061/(ASCE)0733-9429(1997)123:1(58)).
- SEQUEIROS, O. E. Estimating turbidity current conditions from channel morphology: a Froude number approach. *Journal of Geophysical Research*, v. 117, n. 4, p. 1-17, 2012. <http://dx.doi.org/10.1029/2011JC007201>.
- SHIELDS, A. *Anwendung der Aehnlichkeitsmechanik und der Turbelens Forschung auf die Geschiebebewegung*. Berlim: Mitteilungen der Preussische Versuchanstalt für Wasserbau und Schiffbau, 1936.
- SIMONS, D. B.; RICHARDSON, E. V. Forms of bed roughness in alluvial channels. *Journal of the Hydraulics Division, New York*, v. 87, n. 3, p. 87-105, 1961.
- SIMPSON, E. J. *Gravity currents in the environment and the laboratory*. 2nd ed. Cambridge: Cambridge University, 1997. 244 p.
- SOUTHARD, J. B.; BOGUCHWAL, L. A. Bed configurations in steady unidirectional water flows: Part 2. Synthesis of flume data. *Journal of Sedimentary Petrology*, v. 60, n. 5, p. 658-679, 1990. <http://dx.doi.org/10.1306/212F9241-2B24-11D7-8648000102C1865D>.
- SPINELINE, B.; SEQUEIROS, O. E.; GARCIA, M. H.; BEAUBOUEF, R. T.; SUN, T.; SAVOYE, B.; PARKER, G. Experiments on wedge-shaped deep sea sedimentary deposits in mini basins and/or on channel levees emplaced by turbidity currents. Part II. Morphodynamic evolution of the wedge and of the associated bedforms. *Journal of Sedimentary Research*, v. 79, n. 8, p. 608-628, 2009. <http://dx.doi.org/10.2110/jsr.2009.065>.
- VAN DEN BERG, J. H.; VAN GELDER, A. 1993. A new bedform stability diagram, with emphasis on the transition of ripples to plane bed in flows over fine sand and silt. In: MARZO, M.; PUIGDEFÁBREGAS, C. (Ed.). *Alluvial sedimentation*. Boston: Blackwell, 1993. p. 11-21.
- VAN RIJN, L. C. Sediment transport, part III: bed forms and alluvial roughness. *Journal of Hydraulic Engineering*, v. 110, n. 12, p. 1733-1754, 1984. [http://dx.doi.org/10.1061/\(ASCE\)0733-9429\(1984\)110:12\(1733\)](http://dx.doi.org/10.1061/(ASCE)0733-9429(1984)110:12(1733)).
- WINTERWERP, J. C.; BAKKER, W. T.; MASTBERGEN, D. R.; VAN ROSSUM, H. Hyperconcentrated sand-water mixture flows over erodible bed. *Journal Hydraulic Engineering*, v. 118, p. 1508-1525, 1992.
- YALIN, M. S. *Mechanics of sediment transport*. Nova York: Pergamon Press, 1972.

#### Authors Contributions

Débora Karine Koller: achievement of research, experiment's survey and data processing, research design and manuscript writing.

Ana Luiza de Oliveira Borges: research design, contribution and correction of the manuscript.

Eduardo Puhl: research design, contribution and correction of the manuscript.

Rafael Manica: research design, contribution and correction of the manuscript.